Proceedings of the 21st ICSMGE, Vienna, Austria, 14 – 19 June 2026. Pistrol, Adam & Schweiger (eds.)
Published by: ÖGG, Austrian Society for Geomechanics, Salzburg, Austria, ISBN 978-3-9503898-4-5
https://doi.org/10.53243/ICSMGE2026-1039

Experimental and theoretical studies of soil pressure on flexible fences.

Askar Khasanov,
Department of Engineering and Theoretical Mechanics, Samarkand State University, Samarkand, Uzbekistan, uzssmge@gmail.com

Zokhir Khasanov
Geotechnical Department, Geofundamentproject LLC, Samarkand, Uzbekistan, uzssmge@gmail.com

Bekzod Toshmuqumov
Department of Civil Engineering, Samarkand State University of Architecture and Construction, Samarkand, Uzbekistan, bekzod060696@gmail.com

ABSTRACT: This article presents the results of experimental studies of the active pressure of soils on flexible retaining structures. The experiments were carried out in a flat trough with a front glass plate and a rear steel plate. The deflections of the plate and the reaction forces at the end of the plate were measured using a dynamometer. The method proposed by the authors for determining the distribution function of the active pressure based on the deflection of the retaining structure makes it possible to use these results in the design and construction of real retaining structures and to determine more accurately the required stiffness EI depending on the permissible displacements f_x. The experiments established the difference in the effects on the active pressure between gravitational and external forces and their loading forms. A coefficient of difference was determined between the active load E_a and the gravitational as well as external loads calculated using the Kuhlmann design model and the results of the experiments. Phenomenological expressions are proposed that make it possible to determine the parameters of the zone of settlement failures behind the wall and the minimum distance of the influence zone of external forces on the loads applied to the retaining structure.

KEYWORDS: Active pressure function, flexible enclosing structures, deflection of flexible plates, gravitational and external loads.

1 INTRODUCTION

Active pressure function It is known that there are three main methods for determining active soil pressure: analytical method for determining the lateral pressure coefficient using the classical soil strength theory proposed by Coulomb (Craig, 2004; Das, 2004,); the laboratory method for determining the lateral pressure coefficient using the classical soil strength theory of Coulomb-Mohr (Kerisel & Absi, 1990) with the use of triaxial compression devices; experimental methods for determining the active force and pressure in flat troughs. The first and second methods for determining the main design parameter ξ refer to an idealized method, where the stress state is assumed to be homogeneous (given). In accordance with the third method, the reactive horizontal forces p_a are determined in flat troughs by measuring the soil reaction with force dynamometers. Currently, a large number of experimental studies have been conducted by (Khasanov & Khasanov, 2020). The experimental and theoretical method presented by the authors, in contrast to the known ones, additionally allows determining the function of its distribution along the height of the enclosing structure and determining the permissible pressures on the surface and the safe distance from the edge of the retaining wall. A theoretical solution has also been proposed using the classical Coulomb failure theory based on the condition of ultimate equilibrium of the soil, flexible retaining structures, deflection of a flexible plate, gravitational and external loads.

1.1 *Determinations of fence plate rigidity*

Considering that the retaining plate acts not only as a retaining wall but also as an element that allows determining reactive pressures by measuring its deflection, its stiffness was determined experimentally. The stiffness parameter clamped at the bottom of the plate had the following geometric dimensions: plate thickness δ=5.0 mm, width b=219 (260) mm, and force application height h_T =1.03 m. The plate deflection graphs were obtained for a cantilever plate located in a vertical position. The deflection of the plate from a concentrated load is determined by the known Equation (10)

$$f = \frac{T}{EI}\frac{(2l^3 - 3l^2(l-z) + (l-z)^3)}{6} \quad (3)$$

The maximum deflection f at $z = l_T$ at the point of application of the horizontal force T is determined by the expression

$$EI = \frac{Tl_T^3}{3f} = \frac{0{,}06 \cdot 1{,}03^3}{3 \cdot 0{,}04595} = 0{,}475\ kN \cdot m^2 \quad (4)$$

On the other hand, for steel, stiffness is defined as the product of EI

$$EI = E\frac{b \cdot \delta^3}{12} = 2 \cdot 10^9 \cdot \frac{0{,}219 \cdot 0{,}005^3}{12} = 0{,}5018\ kN \cdot m^2 \quad (5)$$

where b; δ is the width and thickness of the curing plate.

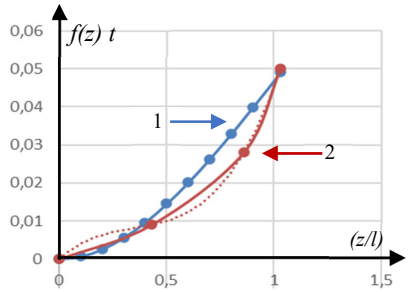

Figure 1. Graphs showing the dependence of the deflection f(z) of the plate on the reduced distance (z/l). 1 and 2 correspond to the experiment and the functions of Equation (1)

A comparison of theoretical and experimental deflection graphs for the plate is shown in Figure 1. As can be seen from the graph, the theoretical results satisfactorily coincide with the experimental ones. This method will be used to determine the

forces and reactive pressure of the soil on the fences, which is discussed below

2 EXPERIMENTAL RESULTS OF THE DEFLECTION OF THE ENCLOSING FLEXIBLE PLATE FROM THE ACTIVE SOIL PRESSURE

The results of the research refer to the determination of the influence of layer-by-layer laying of the build-up soil layer with thickness a and density γ and the results of measuring the reaction force T using a dynamometer installed at a height of 125 mm. The objects of research were: soil №1 – fine sand in air-dry condition with density γ=13,3 kN/m^3 and strength parameters. C=0 , $\varphi = 32^0$ (angle of repose) and soil №2 – crushed stone in an air- dry state with a density of γ =15.3 kN/m^3 and strength parameters c=0, φ =42^0

Research results. Soil №1, soil №2 In the first case, graphs of the deflection of a plate with a displacement restriction from above are shown during its filling with layers with a thickness of a = 30 cm. for the case of a horizontal displacement restriction from above. The measurement results are given in the given coordinates $\frac{1}{2}\gamma\left(\frac{a}{H}\right)$ and $\delta/\left(\frac{z}{H}\right)$. Walls with a filling height of H with a layer of soil and a conditional density of γ^*. $\frac{\gamma^* H}{2} = \gamma\left(\frac{a}{2}\right)$ whence $\gamma^* = \gamma\left(\frac{a}{H}\right)$.

The second argument characterizes the horizontal displacement (deflection) of the plate δ depending on its conditional height $\left(\frac{z}{H}\right)$. In Figure 2 shows graphs of the dependence for both maximum displacements and forces T with the measured value of a dynamometer installed at a height of z = 125 mm. As follows from both graphs, the dependence of the changes in both graphs is nonlinear and obeys a power law.

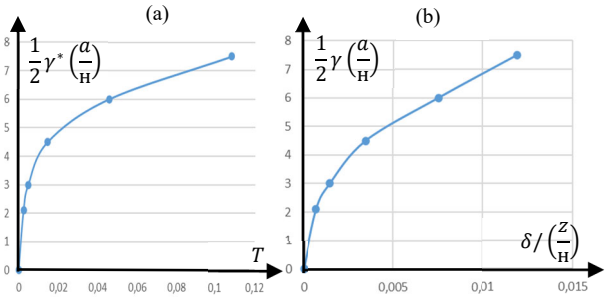

Figure 2. Graphs of dependence of change $\frac{1}{2}\gamma^*\left(\frac{a}{H}\right)$ from T a) and $\frac{1}{2}\gamma^*\left(\frac{a}{H}\right)$ from $\delta/\left(\frac{z}{H}\right)$

2.1 *Test № 2. The results of experimental studies of the deflection function of the enclosing plate s_x and the function of vertical movements of the surface s_z on the amount of active ground*

The results are obtained after filling the tray with sand (soil №1) up to height of 1.25 m. After filling the trough with sand up to the design level of 1.25 m, the threaded screw was slowly unloaded, transferring active pressure to the enclosing slab. After complete unloading of the screw, an area of collapse prism was formed in the contact area of the wall Figure 4., a beyond which an area of subsidence occurred. In Figure 4. b there is a graph of dependence of change of horizontal displacements (deformations) of the enclosing plate (1) s_x and vertical displacements of the ground surface (2) s_z located outside the collapse prism. In the process of the horizontal displacement of the top of the slab causes the ground settlement outside the circulation prism to settle with less intensity, repeating the deflection of the retaining wall.

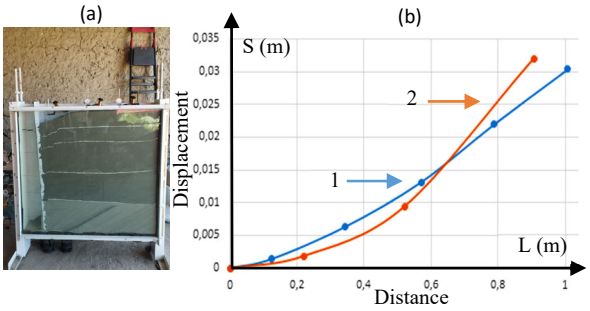

Figure 4. View of the tray, test №. 2. General view of the flume (a). Graphs of dependence of changes in horizontal displacements (deformations) of the enclosing plate (1) and vertical displacements of the ground surface (2) (b)

The measurements made showed that the area of the failed deformations repeat the shape of the deflection and have the following geometric dimensions: $X_z = Ztg\alpha \quad \alpha = \frac{\varphi}{(2{,}5-3{,}5)}$. From where we can conclude that in the case of horizontal displacement or roll of the retaining wall is accompanied with the dynamics of the growth of deformations on its surface and the emergence of failure deformations in the contact area of the wall. If the maximum value of the failure width is taken as a, and the angle of the failure area as $\left(\frac{\varphi}{k}\right)$, the depth of the failure (crack) H can be determined by the equality $tg\left(\frac{\varphi}{k}\right) = \left(\frac{a}{H}\right)$. $H = \left(\frac{a}{tg\left(\frac{\varphi}{k}\right)}\right)$ where k – is a correction factor depending on the type of soil. It is known that such failure deformations and shifts in practice are often observed in collapses, horizontal deformations and rolls of retaining walls, where such deformations also occur on the surface Figure 3., a. Beyond the contour of this boundary tensile stresses occur accompanied by the appearance of longitudinal cracks Figure 3. This expression also characterizes geological processes due to horizontal shears and formation of cracks in the formation of natural canyons. In this case, the depth of the crack will be equal to H*=2H. For example, the width of the canyon is 100 meters. Crack depth

$$H^* = 2\left(\frac{a}{tg\left(\frac{\varphi}{k}\right)}\right) = 2\left(\frac{100}{tg\left(\frac{30}{4}\right)}\right)\frac{200}{0{,}13} = 760\ m \qquad (6)$$

Below we will compare the measured deflections of the plate with traditional methods of calculation.

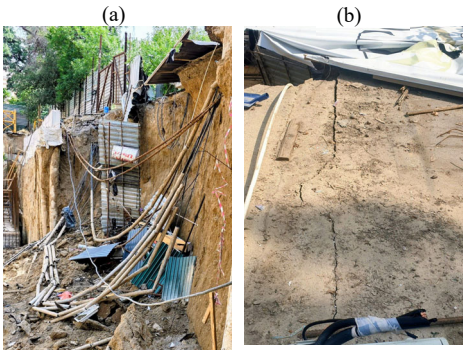

Figure 3. Fragment of the 11 m high retaining wall collapse and the formation of favorable deformations behind the preserved part of the wall (a). Areas of stretching and resulting formation of horizontal cracks (b).

The active soil pressure at the base of the flume P_2 is determined by the Renkin model, known in soil mechanics.

$$P_2 = K_a(P_1 + \gamma \cdot z \cdot b) = tg^2\left(45 - \frac{\varphi}{2}\right)(P_1 + \gamma \cdot z \cdot b) \quad (7)$$

$$P_a = \frac{P_2 h}{2} \quad (8)$$

where γ,z,b are specific weight, height of backfill and width of the flume. For the case of no surface uniformly distributed load P_1=0: Soil №1 P_2=1,12 kN/m.; P_a=0,7 kN and soil №2 P_2=0,93 kN/m.; P_a=0,58 kN.

For theë case of trapezoidal distributed load $P_2 > P_1$ acting horizontally on the console plate its deflection is determined by the known Equation (10)

$$f_x = \frac{P_1}{EI}\left[\frac{h^4}{8} - \frac{h^3(z-h)}{6} + \frac{(z-h)^4}{24}\right] + \frac{P_2 - P_1}{EIh} \cdot \left(\frac{h^5}{30} - \frac{h^4}{24}(z-h) + \frac{(z-h)^5}{120}\right) \quad (9)$$

where z- is calculated from the end of the beam, h is the height of the soil backfill. In particular, at z = 0 and P_1= 0, the maximum deflection will be determined by Equation (9): $f_h = P_2 * h^4/30EI$. However, considering that the unknown in this case is P_2 Equation (9) will be solved with respect to this force. According to the results of tests (soil №1) at the height h=1.25 m, the maximum displacement of the slab f_x=0.08 m was obtained. According to Equation (9), we determine the value of active soil pressure at the base of the slab for: soil №1 P_2=0,5 kPa; E_a=0,32 kN and for soil №2 P_2=0,65 4kPa E_a=0,4 kN. Assuming a triangular shape of the epiphysis distribution, the force is set to $\frac{1}{3}h = \frac{1{,}25}{3} = 0{,}42$ m. From the equation of equality of moments determine the equivalent force T acting from the surface of the envelope $T * h_0 = E_a * 0{,}42$ kN and the force at the level of installation of the dynamometer, respectively $T = \frac{E_a}{l}\left(\frac{h}{3}\right) = \frac{0{,}32*0{,}42}{1{,}25} = 0{,}11$ kN and $T = \frac{0{,}4*0{,}42}{1{,}25} = 0{,}13$ kN. For comparison with the experiments conducted with the measurement of reaction forces for soil №1 measured with a dynamometer showed a force T=0.07 kN. On the basis of the conducted experiments we can make an important conclusion that the calculation of active pressure by the Coulomb-Mohr model (Khasanov & Khasanov, 2020) gives overestimated results. Obviously, this is due to the inhomogeneity of the stress state in the soil located beyond the limits of the retaining wall.

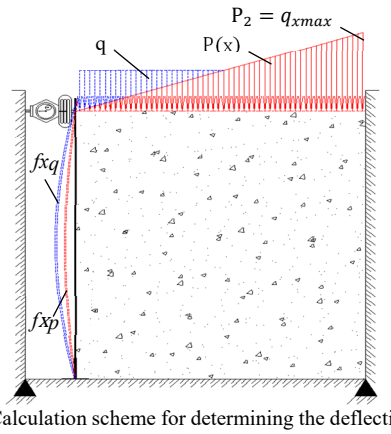

Figure 5. Calculation scheme for determining the deflection of plate f from soil loading with a surface of uniform q and triangular P(x) distributed by loads

2.2 *Test №3, Soil №2 Determining the effects of the type of intense external loads q_x and the gravitational forces of the gunt P_z on the deflection of the enclosing plate f_x and the reaction forces T (for the case of limiting displacements from above),*

Two types of loading were taken as distributed load q_x: uniform and triangular Figure 5.

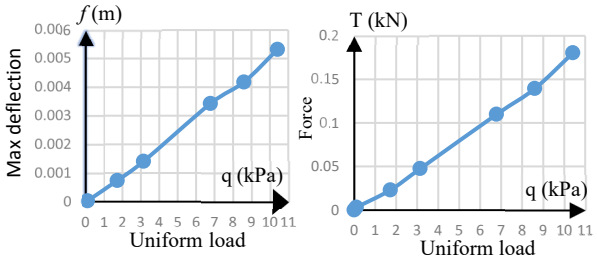

Figure 6. Effect of the magnitude of uniform load q on max deflection and horizontal reactive force. Soil №2.

In both experiments, the conditions of equality $F = q_x lb = q_{xmax}\frac{lb}{2}$. , where $q_{xmax} = 2q_x$.

Case of uniformly distributed load q_x. The distributed loads on the surface were controlled by means of 8 levers with the ratio of arms equal to 1:10. The pressure on the area under each lever was determined by the expression $\sigma_x = \frac{F}{b\Delta l}$ where b=0,22 m, Δl=0,15 m and l=1,03 m, q_x= 0,69; 1,49; 1,89 and 2,29 kN/m. and pressures σ_x= 3,13; 6,77; 8,59; and 10,4 kPa. Figure 6. shows the dynamics of the growth of max deflections f_x and reaction forces T from the growth of stress intensity q_z. As can be seen in this case the graph in contrast to the growth of gravity loads Figure 6. Has a linear, proportional dependence. In the assumption of uniform reaction of active pressure q_x from external q_z and in the assumption with the restriction of displaced from above, we determine the deflection of the strip by Equation (10).

$$f_x = \frac{q_x l^2 x^2}{24EI}\left(\frac{x^2}{l^2} - \frac{5x}{2l} + \frac{3}{2}\right) f_{xmax} = \frac{q_x l^4}{185EI} \quad (10)$$

Same for triangular distributed load

$$f_x = \frac{q_x l^2 x^2}{120EI}\left(4 - 8\frac{x}{l} + \frac{5x^2}{l^2} - \frac{x^3}{l^3}\right) f_{xmax} = \frac{q_x l^4}{418EI} \quad (11)$$

Whence for uniform load q_z by Equation (10) $P_{1x} = \frac{185EI f_{xmax}}{l^4} = 0.27$kN/m. and the obtained result will be compared with Equation (7) $q_x = q_z * \xi$=0.59kN/m.

$\frac{P_1}{q_x} = \frac{0.59}{0{,}27} = 2{,}1$ Uniform load q (kPa).

Case of triangular load and comparison with uniform load Soil №2. Two types of loading intensity were assumed: in the first case for triangular load, the angle factor was assumed to be (0.32) or 180 with Px2q= 0.7 kN/m and q_z= 0.35 kN/m and in the second case (0.51) or 27 0 with Px2q= 1,1 kN/m. (q_z = 0.55 kN/m). The variation of the intensive force function follows the triangular law $P_{2xz} = tg\alpha * x$.

To compare the influence of the type of loading function in both cases, the total forces are selected equal to each other As follows from the presented graphs of plate deflections f_x Figure 7. on its value as well as on the dynamometer readings T there is an influence of loading form more at uniform loading and to a lesser extent triangular loading form. It is connected with the fact that at the triangular form of loading the center of gravity is at the distance l = 1,08 m. At any intensity of loads with the

approach of forces to the envelope both deflection and reaction forces T increase significantly

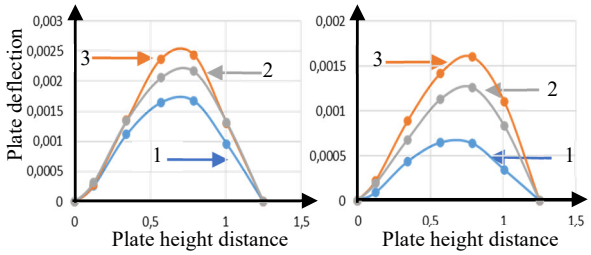

Figure 7. Comparative plots of plate deflection from gravity (1), uniform (3) and triangular (2) distributed load. a - P2-1.35 kN/m and q-0.72 kN/m; b - P2-2.14 kN/m and q-1.15 kN/m.

According to the results of two repeated tests, the results of plate deflections f_{xmax}= 0.01 and 0.0108 were obtained. By Equation (9) we calculate the max value of active pressure at the bottom of the wall: $P_{1x} = f_{xmax}\frac{418EI}{l^4} = 0.01\frac{418{\cdot}0,478}{1,25^4} = 0,82$ and $P_{1x} = f_{xmax}\frac{418EI}{l^4} = 0,0108\frac{418{\cdot}0,478}{1,25^4} = 0,88$ and compare with the active pressure calculated by Equation (3) $q_{xmax} = 2q_z * \xi = 2\cdot 2,29{\cdot}0,259{=}1,2$ kN/m; $\frac{q_{xmax}}{q_x} = \frac{1,2}{0,82} = 1,4;\ 1,36$

Also important is the influence of the proximity of the load to the enclosing slab. For this purpose, special stages of loading were carried out. (Figure 8.) shows the graph obtained from the results of determining the influence of the loading path with uniform intensive loads q_x=0,69;1,49;1,89 and 2,29 kN/m. The loading was built up from the right side of the tray and developed towards the plate. The results in the graph are shown as relative, ratios of force intensity q_x to dynamometer value T (kN), (q/T). As it follows from the graph, the active pressure with approaching (decreasing the distance of the applied force) to the plate grows according to the step law. Minimum distance where there is no influence of load on active pressure $tg\theta = \frac{1,25}{0,9} = 1,25$ or $\theta = 54^0$ which corresponds to the angle of stress dissipation from the external force

$$\alpha = \left(\frac{\pi}{2} - \theta\right) = \left(\frac{\pi}{2} - 54\right) = 36^0 \cong \varphi \qquad (12)$$

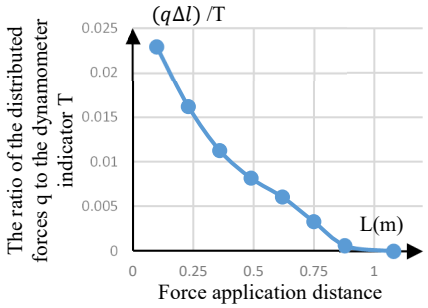

Figure 8. Dependence of the ratio (q/T) on the distance of force application (m)

3 CONCLUSION

1. The design of an experimental flume has been created, where a flexible vertical fence simultaneously allows to determine the reactive active soil pressure function.

2. When the soil behind the retaining wall is filled, the active pressure on the wall grows according to the step law.

3. When the horizontal displacement or roll of the retaining wall occurs outside the retaining wall, failure deformations with abrupt subsidence of the soils may occur. The collapse width a with angle $\alpha = \frac{\varphi}{(2,5-3,5)}$. has been experimentally established. approaching the wall roll. In the process of wall roll on the surface outside the circulation prism, ground settlements with less intensity occur, repeating the roll of the retaining wall.

4. On the basis of the conducted experiments, a phenomenological dependence has been established, which allows to determine the depth of cracking depending on the width of the settling surface. This expression, in general terms, characterizes the geological processes of natural canyons occurrence of their horizontal shear and crack formation.

5. Based on the conducted experiments, we can draw an important conclusion that the calculation of active pressure by the Coulomb-Mohr model (6) gives overestimated results. Obviously, this is due to the inhomogeneity of the stress state in the soil located beyond the limits of the retaining wall.

6. Shows the dynamics of the growth of max deflections f_x and reaction forces T from the growth of stress intensity q_z. As can be seen in this case, the graph in contrast to the growth of gravity loads (Figure 2.) has a linear, proportional dependence.

7. When uniformly distributed forces q_x are applied to the ground surface, the reactive active forces on the retaining wall grow in contrast to the gravitational forces according to the linear law. The plate deflection f_x and the dynamometer readings T are influenced by the loading forms more in case of uniform loading and to a lesser extent by the triangular loading form. This is due to the fact that the center of gravity is at a greater distance under triangular loading than under uniform loading. At any load intensity, as the forces approach the envelope, both deflection and reaction forces T increase significantly according to the step law.

4 REFERENCES

Craig, R.F. 2004. *Craig's Soil Mechanics*. 7th edn. London: Spon Press.

Kerisel, J. and Absi, E. 1990. *Active and Passive Earth Pressure Tables*. 3rd edn. Rotterdam: Balkema.

Das, B.M. 2004. *Principles of Geotechnical Engineering*. 7th edn. Stamford: Cengage Learning.

Milligan, G.W.E. and Houlsby, G.T. (n.d.). *Computerized Techniques for Soil Study*. [Publisher not specified].

ASV Publishing House. 2016. *Geotechnical Handbook: Foundations, Underground Structures*. Moscow: ASV, pp. 588–650.

Khasanov, A.Z. and Khasanov, Z.A. 2020. *Experimental and Theoretical Study of Strength and Stability of Soil*. Boca Raton, London, New York, Leiden: Taylor & Francis Group. 142 p. (A Balkema Book).

Khasanov, A.Z. and Khasanov, Z.A. 2024. 'Stability of natural slopes and determination of pressure from unconsolidated soils on retaining structures', *Journal of Foundations, Mechanics and Geotechnical Engineering*, no. 1.

Rankine, W.M.J. 1857. 'On stability of loose earth', *Philosophical Transactions of the Royal Society of London*, Part I, pp. 9–27.

Saran, S. and Prakash, S. 1968. 'Dimensionless parameters for static and dynamic earth pressure for retaining walls', *Indian Geotechnical Journal*, 7(3), pp. 295–310.

Seed, H.B. and Whitman, R.V. 1970. 'Design of earth retaining structures for dynamic loads', in *Proceedings of the Specialty Conference on Lateral Stresses in the Ground and Design of Earth Retaining Structures*. ASCE, pp. 103–147.

Sherif, M.A., Fang, Y.S. and Sherif, R.I. 1984. 'Ky and Ko behind rotating and non-yielding walls', *Journal of Geotechnical Engineering*, ASCE, 110(1), pp. 41–56.